Elements

Volume 29, Number 1 January 2011

THE NEWSLETTER OF THE CANADIAN GEOPHYSICAL UNION

IN THIS ISSUE

LE BULLETIN DE L'UNION GÉOPHYSIQUE CANADIENNE

CGU-CSAFM 2011 Scientific Meeting

The Joint Meeting between the Canadian Geophysical Union and the Canadian Society of Agricultural and Forest Meteorology will take place May 15-18, 2011, at the Banff Park Lodge at Banff, Alberta. Information on the meeting can be found on the web site http://www.ucalgary.ca/~cguconf. This web site includes information on the technical program, field trips, social programs, student awards, registration, accommodation, and of course, instructions for abstract submission. The deadline for submitting abstracts is February 15. The abstract submission instructions have changed from previous Banff meetings, so please read the instructions carefully before submitting an abstract.

The meeting will have a vibrant technical program that highlights top Canadian and international research contributions, including two sessions in general geophysical areas, four sessions in biogeosciences, four in geodesy, five in hydrology, seven in solid earth studies, two in agricultural and forest meteorology, and one session jointly offered by the CGU-Biogeosciences section and the CSAFM.

The field trip will be a one-day trip to the Columbia Icefield on Sunday May 15.

As always, there will be plenary presentations by leading researchers, an awards banquet, and business meetings of the societies and their sections.

Rencontre Scientifique 2011 de l'UGC et la SCMAF

La Rencontre de l'Union Géophysique Canadienne avec la Société canadienne de météorologie agricole et forestière aura lieu les 15-18 mai 2011 au Banff Park Lodge à Banff, Alberta. Pour informations sur cette rencontre, visitez le site http://www.ucalgary.ca/~cguconf . Ce site contient des informations sur le programme technique, excursions sur le terrain, programmes sociaux, les prix pour les étudiants, l'inscription, l'hébergement, et évidemment les instructions pour la soumission des résumés. La date limite pour soumettre un résumé est le 15 février. Les instructions pour la soumission des résumés ont changé des rencontres précédentes à Banff, alors s'il-vous-plaît lisez les instructions attentivement avant de soumettre un résumé.

La rencontre aura un programme scientifique résonant avec des présentations de première classe de contributions de recherche canadiennes et internationales, incluant deux sessions techniques en géophysique générale, quatre en biogéoscience, quatre en géodésie, cinq en hydrologie, sept en physique des systèmes terrestres, deux en météorologie agricole et forestière, et une session conjointe entre la Section Biogéoscience de l'UGC et la SCMAF.

L'excursion sur le terrain sera d'une journée aux Champs de Glace Colombia dimanche le 15 mai.

Comme toujours, il y aura des présentations plénières par des chercheurs d'avant-garde, un banquet des prix d'excellence, et des rencontres annuelles des sociétés et de leurs sections.

CALL FOR PAPERS / APPEL AUX SOUMISSIONS DE RESUMES

CANADIAN GEOPHYSICAL UNION / UNION GEOPHYSIQUE CANADIENNE
&
CANADIAN SOCIETY OF AGRICULTURAL AND FOREST METEOROLOGY / SOCIETE CANADIENNE DE METEOROLOGIE AGRICOLE ET FORESTIERE

ANNUAL MEETING / RENCONTRE ANNUELLE

May 15 – 18 Mai, 2011

BANFF PARK LODGE, BANFF, ALBERTA

www.ucalgary.ca/~cguconf

Abstract deadline / Date limite pour les résumés: February 15 Février, 2011

Abstracts are solicited in Geodesy, Hydrology, Solid Earth, BioGeosciences, CSAFM and other Geophysical Areas. Preparation and submission details for Abstracts are available at the conference website. For any other information and special requests, please send a message to cguconf@ucalgary.ca

Des Résumés sont sollicités en Géodésie, Hydrologie, Physique des systèmes terrestres, Biogéosciences, SCMAF et autres sujets géophysiques. Les détails pour la préparation et la soumission des Résumés sont disponibles au site Internet de la conférence. Pour tout autre information et demande spéciale, envoyez un message à cguconf@ucalgary.ca

Rod Blais
blais@ucalgary.ca

J. Tuzo Wilson Medal – Call for Nominations

The Executive of the CGU solicits nominations for the J. Tuzo Wilson Medal – 2011. The Union makes this award annually to recognize outstanding contributions to Canadian geophysics. Factors taken into account in the selection process include excellence in scientific and/or technological research, instrument development, industrial applications and/or teaching.

If you would like to nominate a candidate, please contact Dr. Hugh Geiger, Chair of the CGU Awards Committee, Talisman Energy, Calgary AB (Email: HGEIGER@talisman-energy.com). At a minimum, the nomination should be supported by letters of recommendation from colleagues, a brief biographical sketch and a Curriculum Vitae. Nominations should be submitted by February 28, 2011. Additional details concerning the nomination process can be obtained from the Chair of the CGU Awards Committee.

L'exécutif de l'UGC vous invite à suggérer des candidats pour la médaille J. Tuzo Wilson – 2011. L'Union décerne la médaille chaque année "en reconnaissance d'une contribution remarquable à la géophysique canadienne". En choisissant parmi les candidats, on considére les accomplissements en recherches scientifique ou technologiques, aux développements d'instruments, aux applications industrielles et/ou à l'enseignement.

Si vous désirez suggérer un candidat pour cette médaille, s.v.p. contacter Dr. Hugh Geiger, Président du Comité des Prix d'Excellence, Talisman Energy (Email: HGEIGER@talisman-energy.com). Les nominations doivent être supportées de lettres de recommandation de colléques, d'un bref sommaire biographique et d'un Curriculum Vitae. Les nominations doivent être soumises avant le 28 février, 2011. Des détails additionnels concernant le processus de nomination peuvent être obtenus en communiquant avec le Président du Comité des Prix d'Excellence de l'UGC.

Past Wilson Medallists

1978	J. Tuzo Wilson
1979	Roy O. Lindseth
1980	Larry W. Morley
1981	George D. Garland
1982	Jack A. Jacobs
1983	D. Ian Gough
1984	Ted Irving
1985	Harold O. Seigel
1986	Michael Rochester
1987	David Strangway
1988	Ernie Kanasewich
1989	Leonard S. Collett
1990	Gordon F. West
1991	Thomas Krogh
1992	R. Don Russell
1993	Alan E. Beck
1994	Michael J. Berry
1995	Charlotte Keen
1996	Petr Vaníček
1997	Chris Beaumont
1998	Ron M. Clowes
1999	David Dunlop
2000	Don Gray
2001	Roy Hyndman
2002	Doug Smylie
2003	Garry K.C. Clarke
2004	W.R. (Dick) Peltier
2005	Ted Evans
2006	Alan Jones
2007	Herb Dragert
2008	Ming-ko (Hok) Woo
2009	Garth van der Kamp
2010	Nigel Edwards

CGU Young Scientist Award – Call for Nominations

The Executive of the CGU solicits nominations for the CGU Young Scientist Award – 2011. The CGU Young Scientist Awards recognize outstanding research contributions by young scientists who are members of the CGU. Both the quality and impact of research are considered. To be eligible for the award, the recipient must be within 10 years of obtaining their first Ph.D. or equivalent degree. The awards are made by the CGU Executive on the recommendations of a special committee struck for this purpose. The selection committee seeks formal written nominations from the membership, plus letters of support and a current curriculum vitae. Nominations for the CGU Young Scientist Awards may be submitted by CGU members at any time.

If you would like to nominate a candidate, please contact Dr. Hugh Geiger, Chair of the CGU Awards Committee, Talisman Energy, Calgary AB (Email: HGEIGER@talisman-energy.com). The nomination should be supported by three letters of recommendation from colleagues. Nominations should be submitted by February 28, 2011. Additional details concerning the nomination process can be obtained from the Chair of the CGU Awards Committee.

L'exécutif de l'UGC vous invite à suggérer des candidats pour le prix pour Jeune Scientifique de l'UGC – 2011. Les Prix pour Jeunes Scientifiques de l'UGC reconnaissent les contributions exceptionnelles de jeunes scientifiques qui sont membres de l'UGC. La qualité et l'impact de la recherche sont considérés. Pour être éligible pour le prix, le scientifique doit avoir obtenu son premier Ph.D. ou degré équivalent au cours des dix dernières années. Les prix sont accordés par l'Exécutif de l'UGC sur recommendations d'un comité spécial à cette fin. Le comité de sélection sollicite des nominations formelles par écrit des membres de l'UGC, accompagnées de lettres d'appui et d'un curriculum vitae à jour. Des nominations pour les Prix pour Jeunes Scientifiques de l'UGC peuvent être soumis en tout temps par les membres de l'UGC.

Si vous désirez suggérer un candidat pour cette médaille, s.v.p. contacter Dr. Hugh Geiger, Président du Comité des Prix d'Excellence, Talisman Energy, Calgary AB (Email: HGEIGER@talisman-energy.com). Les nominations doivent être supportées de trois lettres de recommandation de colléques. Les nominations doivent être soumises avant le 28 février, 2011. Des détails additionnels concernant le processus de nomination peuvent être obtenus en communiquant avec le Président du Comité des Prix d'Excellence de l'UGC.

Past Winners

2005	Shawn J. Marshall, J. Michael Waddington
2006	No winner
2007	No winner
2008	Brian Branfireun, Scott Lamoureux
2009	Gwenn Flowers, Stephane Mazzotti
2010	Sean Carey

CGU Meritorious Service Award – Call for Nominations

The Executive of the CGU solicits nominations for the CGU Meritorious Service Award – 2011. The CGU Meritorious Service Award recognizes extraordinary and unselfish contributions to the operation and management of the Canadian Geophysical Union by a member of the CGU. All members of the CGU are eligible for this award, although the award is not normally given to someone who has received another major award (e.g. the J. Tuzo Wilson Medal). Nominations for the CGU Meritorious Service Award may be submitted by CGU members at any time. The award is made by the CGU Executive based on recommendations from the CGU Awards Committee, and is based on lifetime contributions to CGU activities.

If you would like to nominate a candidate, please contact Dr. Hugh Geiger, Chair of the CGU Awards Committee, Talisman Energy, Calgary AB (Email: HGEIGER@talisman-energy.com). The nomination should be supported by three letters of recommendation from colleagues. Nominations should be submitted by February 28, 2011. Additional details concerning the nomination process can be obtained from the Chair of the CGU Awards Committee.

L'exécutif de l'UGC vous invite à suggérer des candidats pour le Prix pour Service Méritoire de l'UGC – 2011. Le Prix pour Service Méritoire de l'UGC reconnait les contributions extraordinaires et désintéressées à l'opération et à l'administration de l'Union Géophysique Canadienne par un membre de l'UGC. Tous les membres de l'UGC sont éligibles pour ce prix, sauf que normalement, ce prix n'est pas donné à quelqu'un qui a recu un autre prix important tel que la Médaille Tuzo Wilson. Des nominations pour le Prix pour Service Méritoire de l'UGC peuvent être soumises en tout temps par les membres de l'UGC. Le Prix est accordé par l'Exécutif de l'UGC sur recommendations du Comité des Prix de l'UGC, pour l'ensemble des contributions d'un membre aux activités de l'UGC.

Si vous désirez suggérer un candidat pour cette médaille, s.v.p. contacter Dr. Hugh Geiger, Président du Comité des Prix d'Excellence, Talisman Energy, Calgary AB (Email: HGEIGER@talisman-energy.com). Les nominations doivent être supportées de trois lettres de recommandation de colléques. Les nominations doivent être soumises avant le 28 février, 2011. Des détails additionnels concernant le processus de nomination peuvent être obtenus en communiquant avec le Président du Comité des Prix d'Excellence de l'UGC.

Past Winners

2004	Ron Kurtz
2005	Ted Glenn
2006	J.A. Rod Blais
2007	Ed Krebes
2008	Patrick Wu
2009	Garry Jarvis
2010	Zoli Hajnal

GEODESY SECTION NEWS

Prepared by Patrick Wu

This is a brief summary of the activities of the CGU-Geodesy Section in 2010.

38th Annual Meeting of the CGU, 3rd Joint CMOS-CGU Congress, Ottawa, May 31-June 4, 2010

Besides the 3 scientific sessions, 1) ***Geodesy & Geodynamics***, 2) ***On Advanced Geo-computations and Web Collaboration***, 3) ***Geoid-based North American Vertical Datum***, there was also the ***Global Geodetic Observing System (GGOS) workshop*** which was convened by the Geodetic Survey Division of Natural Resources Canada. In this workshop, Canadian geoscientists discussed how Canada can actively contribute towards its objectives and explored possible future collaboration with interested national and North American agencies involved in Earth and Atmospheric sciences.

Best Student Paper in Geodesy:

The winner of the "Best Student Paper in Geodesy" in 2010 is Panagiotis Vergados (Dept. of Physics and Astronomy, York University). The paper, co-authored with Spiros Pagiatakis, is *"A new technique in retrieving Total Electron Content and second-order ionospheric delays in radio occultation experiments using GPS"*. This paper also won the "CGU Best Student Paper Award" for 2010. The extended abstract of the paper appears below.

Geodesy Section Executive:

The Geodesy Section Executive for the 2010/2011 term was elected during the Annual General Assembly, and it is composed of: Patrick Wu (president , Calgary), Marc Véronneau (vice-president, NRCan), Joe Henton (secretary, NRCan), Mohamed Elhabiby (treasurer, Calgary), JeongWoo Kim (member-at-large, Calgary), Mohammed El-Diasty (member-at-large, York). The past president is Marcelo Santos (UNB).

Geodesy Sessions at the 2011 Meeting

We are all looking forward to the 2011 CGU Annual Meeting to be held in Banff, 15-18 May. This meeting will be a joint meeting with the Canadian Society of Agricultural and Forest Meteorology. There are a number of Geodesy related sessions in the preliminary program. The deadline for abstract submission is February 15, 2011. Details are available on the web site: http://people.ucalgary.ca/~cguconf/2011webs/SessionsE.htm

In addition, at the 2011 meeting, there will be the ***13th Canadian Geoid Workshop***. Please see below for details.

The 13th Canadian Geoid Workshop
Geodetic Survey Division, NRCan
Ottawa, Ontario, Canada

The National Geodetic Survey (USA), Instituto Nacional de Estadística y Geografia (Mexico) and Geodetic Survey Division (Canada) are working towards the definition and realization of new vertical reference System for North America (NAVRS). NAVRS will be an equipotential surface, which will be realized by geoid modeling. It would allow access to the vertical datum through GNSS technologies and allow consistent orthometric heights at any locations across the continent. This new realization of the vertical datum would replace the traditional approach of leveling, which is costly and time-consuming when establishing and maintaining a national datum and limits the access to the datum only where benchmarks are available.

The 13th workshop will focus on three items: 1) Definition of the NAVRS, 2) Theory and data exchange and 3) Monitoring geoid changes. The first item will looks at standards and conventions in establishing the NAVRS. The second item will consist at evaluating theory and data exchange status between national agencies. Finally, the last item consists in establishing cooperation between national agencies and academic institutions for the purpose of realizing an infrastructure for monitoring the geoid variation.

Le 13ième atelier canadien sur le géoïde
Division des levés géodésiques, RNCan
Ottawa, Ontario, Canada

Le National Geodetic Survey (E.U.d'A), Instituto Nacional de Estadística y Geografia (Mexique) et la Division des levés géodésiques (Canada) travaillent ensemble vers la définition et la réalisation d'un nouveau système de référence altimétrique pour l'Amérique du Nord (SRANA). SRANA sera une surface équipotentielle qui se sera réalisé par une modélisation du géoïde. Ceci permettra accès au datum vertical par l'entremisse de la technologie GNSS et permettra des altitudes orthométriques consistantes en tout lieu à travers le continent. Cette nouvelle réalisation du datum vertical remplacera l'approche de nivellement traditionnelle qui est laboureuse et coûteuse pour l'établissement et l'entretien d'un réseau national et qui limite l'accès qu'aux repères altimétriques.

Le 13[ième] atelier portera attention à trois éléments : 1) la définition du SRANA, 2)la théorie et l'échange de données et 3) la surveillance des changements du géoïde. Le premier item regardera aux standards et convention pour la réalisation du SRANA. Le second élément consiste à évaluer la théorie et l'efficacité des échanges de données entre les agences nationales. Finalement, le dernier élément consiste à établir de la coopération entre les agences nationales et les institutions académiques afin de réaliser une infrastructure pour surveiller les variations du géoïde.

BIOGEOSCIENCES SECTION NEWS

Prepared by Altaf Arain, President, CGU Biogeosciences Section
16 December 2010

The Biogeosciences Section had a very successful first annual meeting during CGU- CMOS joint assembly held in Ottawa from May31-June 4, 2010. The Section hosted three sessions with 40 oral and poster presentations. In 2010, the Section also focused on organizational and recruitment activities and elected/selected the following executive members during the Ottawa meeting:

Dr. Altaf Arain (President and Treasure, McMaster University)
Dr. Edward Johnson (Vice President, University of Calgary)
Dr. Carl Mitchell (Secretary, University of Toronto)
Dr. Merrin Macrae (Member at large, University of Waterloo)

A section web page has been developed and can be viewed at http://www.cgu-ugc.ca/BGS_Section/. A listserv has also been created to reach all Section members as well as other researchers related to Biogeosciences. The Section plans to offer student awards for the best student presentation in Biogeosciences during the May 2011 meeting in Banff. The Section also plans to host a joint student conference with the CGU Hydrology Section Eastern Student Conference at McMaster University in 2011.

As of December 2010, the Biogeosciences Section account balance was $862. Most of the Section revenue is from membership fees.

John H. Hodgson

(information provided by Gordon West, University of Toronto)

It is with regret that we would like to inform readers of the passing of John H. Hodgson, a leading Canadian geoscientist of his time. An obituary can be found in the Globe and Mail of Saturday January 15, 2011.

There are probably not many of the present generation of Canadian geophysicists who know of John since he was born in 1913 and has died now at age 98. However, he was the pioneer of crustal seismology in Canada and a key leader of the Seismology section of the Dominion Observatory, the precursor of EMR's Earth Physics Branch and the present Seismology section in the Geological Survey of Canada. According to information found on the Internet, his father E. A. Hodgson was the director of Seismology at the Observatory before him.

John also wrote a two volume history of the Observatory* that was published by the GSC/NRCan. An article on the history of the Observatory can be found in the January 2006 issue of *Elements*.

*Hodgson, J.H.; *The Heavens above and the earth beneath: a history of the Dominion Observatories: volume I, 1905 - 1946;* 1989; and *volume II, 1946 – 1970;* 1994; Geological Survey of Canada Open File, Ottawa.

CGU 2010 Student Paper Competition Winners – Abstracts

The abstracts and expanded abstracts of the winners from the CGU 2010 student paper competition are presented below. For more details, see the July 2010 issue of ELEMENTS, page 30.

Solid Earth Section Award for Best Student Paper:

Winner: Catrina Alexandrakis (Dept. of Geoscience, University of Calgary).

D. M. Gray Award for Best Student Paper in Hydrology (oral presentation):

Winner: Katie Burles (Dept. of Geography, University of Lethbridge).

Campbell Scientific Award for Best Student Poster in Hydrology:

Winner: Laura Brown (Interdisciplinary Centre on Climate Change, University of Waterloo).

Geodesy Section Award for Best Student Paper in Geodetic Research & Education (oral presentation):

Winner: Panagiotis Vergados (Dept. of Physics & Astronomy, York University).

CGU Best Student Paper (all fields of geophysics – oral presentations).

Winner: Panagiotis Vergados (Dept. of Physics & Astronomy, York University).

Honourable Mention: Hilary Dugan (Dept. of Geography, Queen's University).

Precise seismic-wave velocity modeling of the outermost core

Catherine Alexandrakis[*a] and David W. Eaton[b]
Dept. of Geoscience, University of Calgary, 2500 University Drive N.W., Calgary, Alberta, Canada T2N 1N4
[a] alexanc@ucalgary.ca [b] eatond@ucalgary.ca

Earth's shallow core is a region of great uncertainty relating to chemical composition. The outer core is known to be composed of liquid iron and nickel alloyed with ~10% fraction of light elements such as O, S and/or Si. Recent studies have suggested that the outermost core may have a layer enriched in light elements. Identifying such a layer could yield a better understanding of the geodynamo and thermal regime. It is possible to constrain the composition using an accurate seismic velocity model. Thermodynamic and mineral physics experiments commonly use 1-D global velocity models such as *PREM, IASP91* and *AK135*, however these models exhibit significant velocity and density discrepancies in the outermost ~200km of the core.

Here, we apply the Empirical Transfer Function method to obtain precise arrival times for *SmKS* waves. These teleseismic waves propagate as a whispering-gallery mode near the underside of the core-mantle boundary (CMB) and are known to be sensitive to the velocity at their bottoming point. Our dataset mainly samples the uppermost 200km of the outer core, the region with the most velocity uncertainty. Even, global coverage of CMB entry and exit points ensures velocity perturbations from lower mantle heterogeneities are effectively removed.

Of the global reference models *AK135, IASP91* and *PREM*, we find that models *IASP91* and *AK135* do not fit the observed data in the uppermost 200km of Earth's core. Modeling results show a preference towards seismic velocities and depth gradients similar to *PREM*'s in the outermost core. We propose a new, 1-D velocity model called *AE09*. This model has a significantly better fit to the observed data than *PREM*, and a smooth velocity profile that satisfies the adiabatic Adams and Williamson equation. This argues against the presence of an anomalous layer of light material near the top of the core.

Snow melt energy balance in a burned forest stand, Crowsnest Pass, Alberta, Canada.

Burles, K. and Boon, S.
Department of Geography, University of Lethbridge, Lethbridge, AB, T1K 3M4

I. Abstract

The aim of this paper is to quantify differences in snow accumulation, snow surface energy balance, and the timing and magnitude of seasonal snow melt in a burned relative to a healthy forest stand. More snow water equivalent accumulated at peak snow pack in the burned compared to the healthy forest stand. Short-wave radiation was the largest contributor to snow melt in both forest stands with higher inputs in the burned than the healthy site. The removal of forest canopy caused the long-wave flux in the burned site to be lower than in the healthy site. Higher wind speeds resulted in higher sensible and more negative latent heat fluxes in the burned relative to the healthy forest site. Ground heat flux contributions to snow melt were minimal, but were observed to be slightly higher in the burned site which corresponded with warmer ground temperatures and lower soil moisture. The snow pack in the burned stand melted more rapidly; complete snow pack removal occurred seven days sooner than in the healthy site. This study simulated greater snow melt rates in the burned stand than those observed in mountain pine beetle (MPB) killed stands five years after death, and in the lower range of those observed in cleared forest stands. Stand scale research results can be used to parameterize numerical models designed to simulate watershed scale runoff response to forest disturbance.

II. Introduction

Forests are subject to a range of land uses and natural disturbances that result in a mosaic of stand types across watersheds (Jost *et al.*, 2007). Southwestern Alberta (AB) has seen a mean annual temperature increase of 2°C in the last century (Schindler and Donahue, 2006). Predicted shifts in climate may increase the susceptibility of forest environments to natural disturbances such as insect infestation and wildfire, and associated anthropogenic disturbances such as salvage harvesting. Forest disturbance ultimately opens the forest canopy; however, specific structural impacts vary between disturbance types, with different effects on snow processes. The forest canopy is completely removed in cleared forests, whereas in burned and MPB killed stands the canopy retains dead standing trees that continue to intercept snowfall and shortwave radiation, and decrease wind speeds. In MPB killed stands needles are shed to the snow and ground surface, but some needles and small branches remain intact. Burned forest stands are a unique disturbance type, where needles and small branches are completely removed and all that remains are dead standing trunks and branches. While differences in snow melt processes are well understood between forests and clearcuts (Winkler *et al.*, 2005), the effects of natural disturbance are still largely unknown, although this is changing with recent studies evaluating MPB effects on snow processes (Boon, 2009). No research has been conducted to quantify the effects of forest cover change following wildfire on snow accumulation, snow surface energy balance, and the timing and magnitude of seasonal snow melt.

Wildfire frequency and area burned in Canada have been increasing since the early 20th century (Podur *et al.*, 2002). Partial or total removal of the forest canopy by wildfire reduces the interception capacity of forest environments (Farnes and Hartmann, 1989), increasing snow accumulation in burned forest stands. The snow surface energy balance is also significantly affected by forest canopy characteristics given the canopy's ability to absorb and reflect incoming shortwave radiation, emit long-wave radiation, and shade the snow surface causing lower snow surface albedo (Link and Marks, 1999). Reduced forest canopy increases short-wave radiation reaching the snow surface, increases wind speeds, increases vapour pressure and temperature gradients between the snow surface and the atmosphere, decreases long-wave radiation emissions towards the snow surface, and subsequently enhances the energy available for snow melt. The purpose of this research is to quantify the effects of wildfire on snow melt energy balance and seasonal timing of snow melt in a burned versus a healthy mature forest stand in the Crowsnest Pass, AB.

III. Study Site

Two north-facing, 2500 m^2 stands at the northern edge of the 2003 Lost Creek wildfire boundary in the Crowsnest Pass, in the Oldman River Basin headwaters (Figure 1), were selected for study. The healthy (control) stand is at 1680 m elevation and is representative of the mature forest cover of the region. The burned stand is ~1 km away at 1775 m elevation, and is representative of the most severely burned forest in the Lost Creek fire area. Meteorological data collected in both stands (*IV. Methods*) indicate that they respond to similar large-scale weather conditions. The dominant tree species is subalpine fir (*Abies lasiocarpa*), with a small portion of white spruce (*Picea glauca*) and lodgepole pine (*Pinus contorta var. latifolia*) in both sites. Average tree height and diameter at breast height (DBH) is similar for both stands; however, tree density and basal area are 60% lower in the burned stand indicating the greatest variation between stands can be attributed to differences in canopy structure.

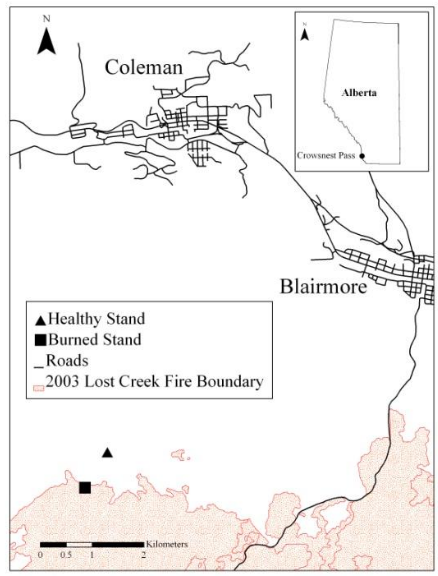

Figure 1: Study area region and location of the forest stands

Environment Canada's nearest climate station to the study area is located at Coleman, AB, at an elevation of 1341 m. This station's annual average (1971-2000) air temperature is 3.5°C, and it receives approximately 57.7 cm of water equivalent precipitation per year, 30% occurring as snowfall.

IV. Methods

In October 2008, a 10 m Campbell Scientific (CSC) meteorological tower was installed in each of the healthy and burned forest stands to collect 20 min average, and 24 hr maximum and minimum data during the snow melt period. Measurements include air pressure, air temperature, snow surface temperature, sonic air temperature, relative humidity, wind speed, ground heat flux, soil temperature, volumetric soil water content, incoming short-wave and long-wave radiation, snow surface albedo, and snow depth. Peak snow accumulation and snow pack depletion were monitored by measuring snow water equivalent (SWE). Snow density measurements were collected at 36 permanent snow survey sites located on a 50 x 50 m grid in each 2,500 m^2 stand. Snow depth measurements (n = 121) were collected at 5 m intervals within the same sampling grid and were multiplied by the density measurements to determine stand average SWE. Snow survey measurements were collected in mid February, early March, and weekly throughout the spring snow melt period.

Canopy density parameters were calculated using hemispherical photos taken in close proximity to the meteorological stations using a Canon EOS 5D digital SLR camera with fullframe sensor and a Sigma 180° true fisheye lens on a leveled tripod. Hemi-photos were processed using Side-Look detection edge software (Nobis, 2005), and Gap Light Analyzer (GLA) (Frazer *et al.*, 1999) to determine the sky view factor (τ_L: fraction of hemisphere visible from beneath the canopy). Canopy transmissivity (τ_c) of incoming short-wave radiation ($K\downarrow$) in the burned stand was assumed to equal τ_L because there were no needles or branches to restrict transmissivity of incoming short-wave radiation ($K\downarrow$). τ_c was calculated in the healthy stand using a 60-day average ratio of 20-minute measurements of $K\downarrow$ in the burned stand to $K\downarrow$ measured beneath the healthy forest canopy.

Energy balance components were simulated hourly for each stand during the snow melt period (April 1- May 25) using:

$$Q_m = L^* + K^* + SHF + LHF + GHF \tag{1}$$

where Q_m is the total energy available for melt, L^* is net long-wave radiation, K^* is net short-wave radiation, *SHF* is sensible heat flux, *LHF* is latent heat flux, and *GHF* is ground heat flux (all terms in W m^{-2}). Advective energy (energy supplied to the snow pack by rainfall) was not considered as it was not observed during the 2009 snow melt period. Additionally, internal snow pack processes are not physically represented however, cold content was calculated and incorporated empirically into the simulation to account for the energy required to warm the snow pack to the melting point (0°C).

Model performance was assessed by comparing the rate and timing of continuous records of observed versus simulated melt. Observed SWE was derived from the continuous snow depth record and averaged snow survey density measurements. Goodness-of-fit between observed and simulated SWE was determined using three quantitative measures of performance: coefficient of determination (r^2), coefficient of efficiency (E), and root mean square error (RMSE) (Confalonieri *et al.*, 2010).

V. Results and Discussion

Simulation performance is summarized in Table 1. Coefficients of determination indicate that the simulation explains a high proportion of the variance in measured SWE. The simulation slightly over simulates high snow melt rates (slope > 1), while the negative y-intercepts suggest either an over simulation of low melt rates, or the failure to consider snow redistribution in the simulation: over simulation of snow melt could actually be snow removed by wind scour. High E values indicate the predictive ability of the simulation is high. The date of complete snow pack

Table 1: Comparison of simulated vs. measured SWE (Apr 1 - May 25)

	Burned	**Healthy**
n (hours)	1271	1439
r^2	0.94	0.96
Slope	1.09	1.10
Intercept	-0.33	-2.65
E	0.81	0.94
RMSE (cm)	2.48	1.01
Date of snow pack removal		
Measured	143	151
Simulated	141	151

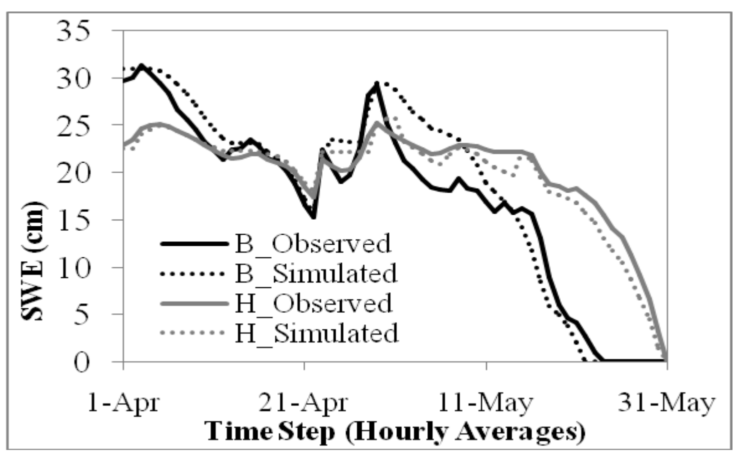

Figure 2: Simulated and observed snow water equivalent (Apr 1 - May 31)

removal was simulated accurately in the healthy stand, but in the burned stand was simulated two day sooner than observed (Figure 2).

Maximum observed SWE was 5.8 cm greater in the burned than in the healthy stand. SWE peaked in both forest stands just before April 1st and the snow melt period lasted ~53 and 60 days in the burned and healthy stands, respectively. Differences in micrometeorological variables and forest structure parameters between stands (Table 2) resulted in larger energy balance fluxes in the burned than the healthy stand (Figure 3). Approximately 83% more energy

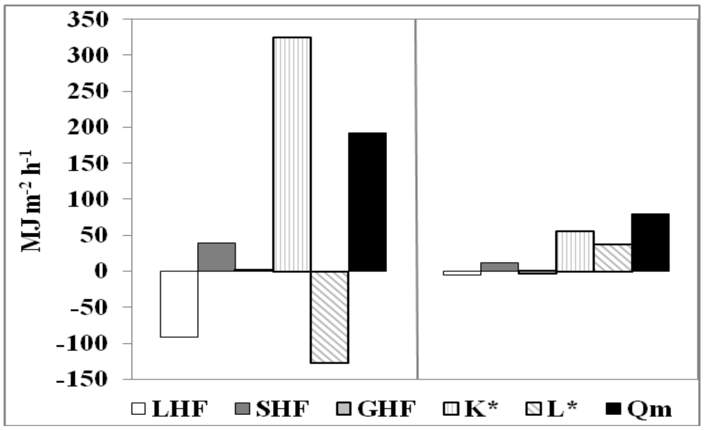

Figure 3: Cumulative (Apr 1 - May 25) energy balance components: burned (left) and healthy (right) forest stand

Table 2: Average meteorological conditions (Apr 1 - May 25) and forest structure parameters at both sites

	Burned	Healthy
T_{ss} (°C)	-3.5	-1.5
T_a (°C)	1.5	1.8
μ (m s^{-1})	1.2	0.4
τ_c	0.82	0.085
τ_L	0.82	0.18
α	0.62	0.35
T_s (°C)	1.1	0.1
VWC (%)	13	30

was available for melt in the burned relative to the healthy stand over the melt period. Snow melt was largely driven by *K** and *SHF* in the burned stand, and a combination of *K**, *L**, and *SHF* in the healthy stand. In the burned stand, greater temperature gradients between the snow surface (T_{ss}) and overlying air (T_a), as well as greater wind speeds (μ) resulted in more significant turbulent fluxes: *LHF* was 175% higher and *SHF* was 63% lower than in the healthy stand. *K** was the largest contributor to Q_m in both stands. The lack of forest canopy resulted in 162% more $K\downarrow$ reaching the snow surface (higher τ_c) and 65% higher albedo (α) in the burned relative to the healthy stand. Consequently, simulated *K** was more sensitive to differences in τ_c than α. More $K\downarrow$ was absorbed by the forest canopy (lower τ_L) in the healthy stand, resulting in more long-wave radiation emission from the forest canopy and tree trunks ($L\downarrow$) onto the snow surface, contributing to melt. In the burned stand, colder T_{ss} caused lower long-wave emissions from the snow surface ($L\uparrow$) than the healthy, which were not compensated by long-wave emissions from the forest canopy (higher τ_L) given the burn severity. Thus almost negligible $L\downarrow$ values and higher $L\uparrow$ resulted in negative *L** and subsequently reduced Q_m in the burned stand. *GHF* did not significantly contribute to Q_m; however, *GHF* was 222% higher in the burned stand due to warmer soil temperatures (T_s), and lower volumetric water content (VWC) (Table 2). SWE calculated using Q_m gave average melt rates for the period of rapid melt (May 1-25) of 14 and 6 mm d^{-1} in the burned and healthy stands, respectively. This resulted in complete snow pack removal seven days sooner in the burned relative to the healthy forest stand.

Maximum observed SWE was 19% greater in the burned than in the healthy stand, similar to observations from cleared and MPB killed forest stands (Winkler *et al.*, 2005; Boon, 2009). Comparison of the ratio of snow melt rates in disturbed versus healthy forest stands indicates that the burned stand (0.67) is significantly higher than MPB killed stands (0.14-0.17)

(Boon, 2009), but is comparable to the lower range of cleared forest stands (0.3-3) (Pomeroy and Granger, 1997; Winkler *et al.*, 2005; Lopez-Moreno and Stähli, 2008).

VI. Conclusion

Wildfire removes forest canopy which subsequently increases snow accumulation and affects the rate and timing of snow melt. Burned stands have more energy available for snow melt which is derived from more positive sensible heat flux, ground heat flux, and net short-wave radiation than healthy stands. Because wildfire completely removes the forest canopy, snow melt rates are higher than those in MPB-killed forest stands, and are closer to those reported for cleared forest areas. Although results are comparable to cleared forest stands, they will always be lower as standing dead trees in burned forest stands attenuate incoming shortwave radiation, wind speed, temperature, snow accumulation, and increase incoming long-wave radiation at the snow surface. Additional years of data collection are necessary to assess the effects of inter-annual hydro-climatic variability on snow melt energy balance in burned forest stands.

VII. References

Boon, S. 2009. 'Snow ablation energy balance in a dead forest stand', Hydrol. Process. 23, 2600-2610.

Confalonieri, R., Bregaglio, S., and Acutis, M. 2010. 'A proposal of an indicator for quantifying model robustness based on the relationship between variability of errors and of explored conditions', Ecol. Model. 21, 960-964.

Farnes, P.E., and Hartmann, R.K. 1989. 'Estimating the effects of wildfire on water supplies in the Northern Rocky Mountains'. Proc 57th Western Snow Conf., CO, Apr 18-20, 90-99.

Frazer, G.W., Canham, C.D., and Lertzman, K.P. 1999. 'Gap light analyzer (GLA), Version 2D0: Users manual and program documentation', Burnaby: Simon Fraser University and Millbrook: Institute of Ecosystem Studies.

Jost, G., Weiler, M., Gluns, D.R., and Alila, Y. 2007. 'The influence of forest and topography on snow accumulation and melt at the watershed-scale', J. Hydrol. 347, 101-115.

Link, T.E., and Marks, D. 1999. 'Point simulation of seasonal snow cover dynamics beneath boreal forest canopies', J. Geophys. Res. 27, 841-857.

López-Moreno, J.I., and Stähli M. 2008. 'Statistical analysis of the snow cover variability in a subalpine watershed: assessing the role of topography and forest interactions', J. Hydrol. 379–394.

Nobis, M., and Hunkizer, U. 2005. 'Automatic thresholding for hemispherical canopy-photographsbased on edge detection', Agric. For. Meteor. 128, 243-250.

Podur, J., Martell, D. L.,and Knight, K. 2002. 'Statistical quality control analysis of forest fire activity in Canada', Can. J. Forest Res. 32, 195–205.

Pomeroy JW, and Granger RJ. 1997. 'Sustainability of the western Canadian boreal forest under changing hydrological conditions—I—snow accumulation and ablation', IAHS Publication. 240: 237–242.

Schindler, D.W., and Donahue, W.F. 2006. 'An impending water crisis in Canada's western prairie provinces', P. Natl. Acad. Sci. USA. 103, 7210–7216.

Winkler, R., Spittlehouse, D.L., and Golding, D.L. 2005. 'Measured differences in snow accumulation and melt among clearcut, juvenile, and mature forests in southern British Columbia', Hydrol. Process. 19, 51-62.

Modelling lake ice thickness – a comparison of measured and simulated ice thickness from the 2008-2009 ice season in Churchill, Manitoba

Laura C. Brown and Claude R. Duguay
Interdisciplinary Centre on Climate Change (IC3), University of Waterloo, ON
lcbrown@uwaterloo.ca

Introduction

Lakes comprise a large portion of the surface cover in Northern Canada forming an important part of the cryosphere, with the ice cover both playing a role in and responding to climate variability. In northern regions where observational data is sparse, lake ice models are ideal as they can provide valuable information on ice cover regimes. One important benefit of modelling is the ability to simulate ice conditions under future climate scenarios and examine any changes to the break-up/freeze up, thickness and ice composition (black ice vs. snow ice) that may occur. However, before future conditions can be explored, models need to be validated against current conditions. Validation of modelled ice thickness presents unique difficulties as frequent sampling is not logistically feasible in remote locations and ice thickness on small lakes is not easily obtainable from satellite imagery. The objective of this study is to examine the effectiveness of the Canadian Lake Ice Model (CLIMo) at simulating ice thickness compared to *in situ* ice thickness measurements using upward-looking ice profiling sonar.

Study Area and Methodology

The selected lake for this study, Malcolm Ramsay Lake (Lake 58), is situated within the Hudson Bay Lowlands in a forest-tundra transition zone near Churchill, Manitoba (58.72°N, 93.78°W). The lake covers an area of 2 km^2 with a mean depth of 2.4 m (maximum depth of 3.2 m) (Duguay *et al.*, 2003).

A one-dimensional thermodynamic model (CLIMo) was used to simulate ice cover for the lake throughout the 2008-2009 winter season. A detailed description of CLIMo can be found in Duguay *et al*. (2003). In order to account for snow redistribution on the lake ice surface, the model was run using a series of snow cover scenarios (0 -100% of the on-shore snow cover depths).

The model was driven by on-shore meteorological data from a Campbell Scientific Automated Weather Station (AWS). Input data for the model included air temperature and relative humidity (HC-SC-XT Temperature and Relative Humidity probe), wind speed (RM Young Wind Monitor) and snow depth (SR50A Sonic Ranging Sensor). In addition to the AWS data, cloud cover data was extracted from the MODIS Cloud Product (1-km, percentage total cloud cover) for the coordinates coinciding with the AWS. A snow density value of 246.1 kgm^{-3} was used in model simulations, determined from previous snow sampling at the study site (Duguay *et al*., 2002). A Campbell Scientific digital camera (CC640 Digital Camera) was installed on the AWS, capturing hourly images of the lake to allow for on-site observations of the ice processes.

In order to validate and improve the model results, *in situ* measurements of the ice cover formation and decay were obtained using a Shallow Water Ice Profiling Sonar (SWIPS) - an upward-looking sonar device installed on the bottom of the lake within the field of view of the digital camera. The SWIPS collected acoustic ranges every second, creating a continuous data set of the ice cover season. Output from the SWIPS includes water level (from a built-in pressure transducer combined with on-shore barometric pressure at the AWS, 61205V Barometric Pressure Sensor), water temperature at the sensor, and distance to the bottom of the ice cover. Frequent onboard measurements (every 60 seconds) of instrument tilt allow for the acoustic range to be corrected to vertical, and when combined with the corrected water levels, permit the calculation of the overall ice thickness.

Additionally, field measurements were obtained weekly during the spring of 2009 (April 13 until June 27) consisting of the on-ice snow depth, thickness of the snow-ice layer (if present) and the total ice cover thickness.

Results and Discussion

Ice formation was detected by the SWIPS on Oct. 26, 2008 (with a brief ice cover noted on Oct 10/11) and clearly detected by the digital camera on Oct. 27 (*Figure 1a, Figure 2*). The ice thickened throughout the season until it exceeded the lower limit detectable by the SWIPS (0.5 m above the sensor) on March 21, 2009. However, field measurements allowed for the maximum ice thickness to be determined before the decay of the ice cover took place between June 10 and July 9. Visible ponding, shushing and ice decay were seen in the camera imagery from June 11 – July 9, with the first open water detected on June 26 (*Figure 1c*). Field measurements of on-ice snow thickness showed the absence of snow cover on the lake ice by June 10 (coinciding with the onset of ice break-up).

Figure 1. (a) Ice cover formation, (b) snow redistribution on the ice surface, and (c) ice break-up in progress with open water and slush visible on the ice surface.

Model simulations were generated using the following snow cover scenarios: 0%, 5%, 10%, 25% and 100% of the on-shore snow cover (*Figure 2*). All simulations had ice formation occur on Oct. 26. Ice formation from the 100% snow cover scenario formed thicker ice immediately, whereas ice thickening with snow cover less than 25% was delayed by approximately two weeks. The 100% snow scenario simulated the initial ice thickening well until Nov. 23, at which point the simulated ice thickening from this scenario was more gradual than measured. After Nov. 23, the 5% snow cover scenario simulated the thickening of the ice cover very well. This shift in the thickening regime is likely related to the substantial redistribution of the initial snow cover that occurred from Nov. 20 to Nov. 21 (*Figure 1b*).

While the 5% snow scenario simulated the actual thickening of ice through the winter to early April, field measurements showed the ice to be thicker than that produced by the model. During this time several snowfall events occurred which increased the snow depth on the ice well beyond that simulated in the 5% scenario (*Figure 2*) and increased the thickness of the snow ice layer. Virtually no snow ice was generated by the 5% snow scenario, however nearly 0.3 m was present at the onset of melt (~June 10) exceeding that simulated by the 25% snow cover scenario. All simulations overestimate the rate of ice decay (from snow-free ice cover to no ice), which is a likely result of the exclusion of snow-ice in the albedo parameterization in CLIMo (Jeffries *et al.*, 2005). The underestimation of the simulated ice thickness (with the exception of the 0% snow cover simulation), combined with the poorly simulated amounts of snow ice formation and overestimated rate of ice thinning, results in break-up occurring 2-3 weeks prior to the observed dates (simulated: June 19-26, observed: July 9).

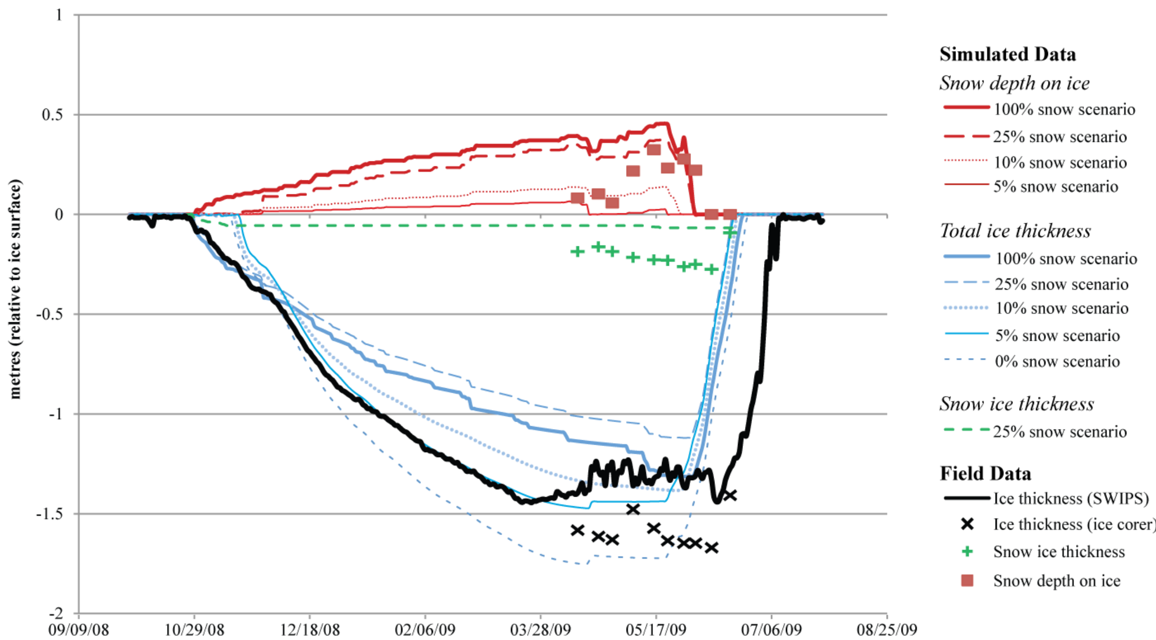

*Figure 2.*Comparison of ice thickness, snow-ice thickness and on-ice snow depth between measured and simulated values.

In order reduce the discrepancies between the observed and simulated ice cover thickness (and hence the timing of break-up), further simulations will be conducted using field data collected during the 2009-2010 season. This will include frequent snow depth and density measurements on the ice surface allowing for a more accurate representation of the seasonal snow changes. Improvements to the albedo parameterization and an exploration into the discrepancies of snow ice formation are expected to produce more reliable simulations for this environment.

References

Duguay, C.R., Flato, G.M., Jeffires, M.O., Ménard, P., Morris, K. and Rouse, W.R. 2003. 'Ice-cover variability on shallow lakes at high latitudes:model simulations and observations', Hydrological Processes, 17, 3465-3483.

Duguay, C.R., Pultz, T.J., Lafleur, P.M., Drai, D. 2002. 'RADARSAT backscatter characteristics of ice growing on shallow sub-arctic lakes, Churchill, Manitoba, Canada', Hydrological Processes 16, 1631-1644.

Jeffries, M.O., Morris, K., Duguay, C.R. 'Lake ice growth and decay in central Alaska, USA: observations and computer simulations compared', Annals of Glaciology, 40, 1-5.

A new technique in retrieving Total Electron Content and second-order ionospheric delays in radio occultation experiments using GPS

Panagiotis Vergados* and Spiros D. Pagiatakis
Department of Physics and Astronomy, York University
4700 Keele Street, Toronto, Ontario M3J 1P3, Canada. *vergados@yorku.ca, spiros@yorku.ca

Abstract
This paper introduces a novel approach for the assessment of the second-order ionospheric effect on Global Positioning System (GPS) radio occultation (RO) data products. We present a new linear combination between dual frequency GPS observables, which retrieves slant total electron content (STEC) free from the second-order ionospheric effect. Our STEC values differ from those obtained by independent techniques by a maximum of 3 Total Electron Content Units (TECU). Additionally, we compute second-order ionospheric delays in RO experiments in near-real time, without using geomagnetic and ionospheric models. First estimates show that second-order ionospheric delays in RO experiments falls within the range [-10, -8] mm. The proposed methods have the potential to be implemented in state-of-the-art GPS processing packages such as, BERNESE and GYPSY improving the current observation accuracy in a broad spectrum of geodetic studies.

Introduction
Radio occultation (RO) is a technique used for remote sensing the Earth's atmosphere since 1995 [*Anthes et al.,* 2008]. Receivers on board Low Earth Orbiters (LEO) record both, the amplitude and phase of the transmitted dual frequency (L_1: f_1=1.57542 GHz; L_2: f_2=1.22760 GHz) GPS signals traversing the Earth's ionosphere and neutral atmosphere, as the GPS satellites set or rise behind the Earth's limb [cf., Fig. 1].

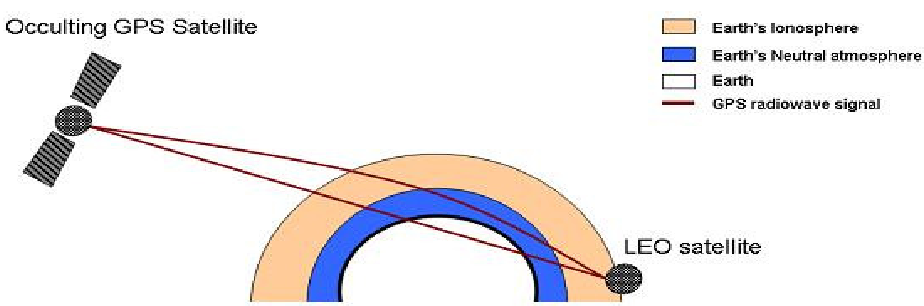

Figure 1: A schematic drawing of the GPS radio occultation technique. The red lines represent the GPS radio signal propagation in the presence (curved) and in the absence (straight line) of the Earth's atmosphere.

To remove the ionospheric contribution from the GPS measurements, *Guier and Weiffenbach* [1960] suggested forming the ionosphere-free linear combination between dual frequency GPS observables. Nevertheless, second- and higher-order ionospheric residuals remain uncorrected, even after forming the ionosphere-free linear combination, which limit the accuracy of GPS measurements.

Particularly, the achieved accuracy in point positioning, after removing the first-order ionospheric effect from the GPS observables, is at the centimeter-level. However, recent GPS applications including monitoring plate tectonic motion, crustal deformation and atmospheric sounding require millimeter-level accuracy in receiver and satellite positions [*Bos,* 2005]. Hence, the accurate assessment of the potential impact of the second-order ionospheric effect on GPS applications gained the interest of the scientific community. *Kedar et al.* [2003] and *Morton et al.* [2009] estimated the second-order ionospheric effect for ground-based receiver positioning between 1 mm and 10 mm. However, information about the magnitude and impact of the second-order ionospheric effect on RO observables and derived products has not yet received any attention, despite the GPS advancements in geodetic applications, space weather forecasting and climatological model development [*Anthes et al.,* 2008].

This paper introduces a new algorithm which is able to determine the second-order ionospheric delay in RO experiments in near-real time. Applying the proposed algorithm in RO experiments, we also propose a new technique to estimate RO STEC free from the second-order ionospheric effect. The testing of this algorithm is performed by the use of level-1b observational data provided by the Constellation Observing System for Meteorology, Ionosphere and Climate (COSMIC) Data Analysis and Archive Centre (CDAAC).

Methodology

Taking into consideration the second-order ionospheric effect, we can model the L_1 and L_2 GPS phase measurements, using the observation equations:

$$(L_1-\rho)\cong-\frac{40.3}{f_1^2}\cdot STEC_1-\frac{K\cdot\left\langle B_{\parallel}\right\rangle_1}{f_1^3}+\lambda_1 N_1+b^{GPS,L_1}+b_{LEO,L_1}+mp_{L_1}+\varepsilon_{L_1} \tag{1}$$

$$(L_2-\rho)\cong-\frac{40.3}{f_2^2}\cdot STEC_2-\frac{K\cdot\left\langle B_{\parallel}\right\rangle_2}{f_2^3}+\lambda_2 N_2+b^{GPS,L_2}+b_{LEO,L_2}+mp_{L_2}+\varepsilon_{L_2} \tag{2}$$

where ρ is the GPS–LEO line-of-sight (LoS) (m), $STEC_i=\int_{GPS}^{LEO} n_e^{(i)} ds$ is the slant total electron content (TECU) and $\left\langle B_{\parallel}\right\rangle_i=\int_{GPS}^{LEO} B\cos\theta\cdot n_e^{(i)}ds$ is the geomagnetic field (T/m^2) weighted by the electron number density n_e along the GPS–LEO propagation path, with i=1,2 representing the two different frequencies. λ_1, λ_2 (m), N_1, N_2, b^{GPS,L_1}, b^{GPS,L_2}, b_{LEO,L_1}, b_{LEO,L_2}, mp_{L_1}, mp_{L_2}, and ε_{L_1}, ε_{L_2} are the wavelengths, the integer carrier-phase ambiguities, the inter-frequency biases, multipath and noise at L_1, L_2 channels, respectively.

Traditionally, RO STEC is computed by differencing the L_1 and L_2 GPS observables [cf., Eqs. (1,2)]. This approach is currently used by CDAAC to estimate calibrated RO STEC along the line of sight (LoS) between a GPS and a LEO satellite [*Hajj et al.,* 2000]:

$$STEC=\frac{f_1^2 f_2^2}{40.3(f_1^2-f_2^2)}(L_1-L_2) \tag{3}$$

Syndergaard [2002] suggested a different approach in estimating RO STEC by accounting for the ionospheric bending and/or dispersion effects through the following equation:

$$STEC=\frac{f_2^4 L_2-f_1^4 L_1}{40.3(f_1^2-f_2^2)} \tag{4}$$

However, Eqs. (3, 4) do not account for the ray path splitting between the L_1 and L_2 signals, disregard the second-order ionospheric effect as well as the L_1 and L_2 carrier-phase ambiguities, local multipath, background ionospheric noise, scintillation effects and receiver clock errors.

Our research focuses on improving the RO STEC estimates at all conditions thus, we consider the ray path splitting between the L_1 and L_2 GPS signals. To provide more accurate RO STEC estimates, we propose computing the STEC over both, the L_1 and L_2 signal paths and then form a new STEC linear combination similar to that of the ionosphere-free linear combination thus, avoiding any unjustified assumptions as to which path the RO-derived STEC should be assigned on. Under these assumptions, we solve Eqs. (1, 2) with respect to $STEC_1$ and $STEC_2$:

$$STEC_1 = -\frac{(L_1-\rho)}{40.3}\cdot f_1^2 - \frac{K\cdot\langle B_\parallel\rangle_1}{40.3\cdot f_1} + \frac{f_1^2}{40.3}\cdot\left(\lambda_1 N_1 + b^{GPS,L_1} + b_{LEO,L_1} + mp_{L_1} + \varepsilon_{L_1}\right), \tag{5}$$

$$STEC_2 = -\frac{(L_2-\rho)}{40.3}\cdot f_2^2 - \frac{K\cdot\langle B_\parallel\rangle_2}{40.3\cdot f_2} + \frac{f_2^2}{40.3}\cdot\left(\lambda_2 N_2 + b^{GPS,L_2} + b_{LEO,L_1} + mp_{L_1} + \varepsilon_{L_1}\right). \tag{6}$$

Because the ray path splitting between the L_1 and L_2 GPS signals in the ionosphere is very small, we do not expect the geomagnetic field to be different between the two paths. Hence, by forming a linear combination between the $STEC_1$ and $STEC_2$, we obtain:

$$\begin{aligned} STEC = {} & \frac{STEC_1\cdot f_1^2 - STEC_2\cdot f_2^2}{f_1^2-f_2^2} - \frac{K\cdot\overline{B_\parallel}\cdot\left(STEC_1\cdot f_1 - STEC_2\cdot f_2\right)}{40.3\cdot\left(f_1^2-f_2^2\right)} + \\ & + \frac{1}{40.3\cdot\left(f_1^2-f_2^2\right)}\cdot\left[\left(\lambda_1 N_1 f_1^4 - \lambda_2 N_2 f_2^4\right) + \left(b^{GPS,L_1} f_1^4 - b^{GPS,L_2} f_2^4\right) + \right. \\ & \left. + \left(b_{LEO,L_1} f_1^4 - b_{LEO,L_2} f_2^4\right) + \left(mp_{L_1} f_1^4 - mp_{L_2} f_2^4\right) + \left(\varepsilon_{L_1} f_1^4 - \varepsilon_{L_2} f_2^4\right)\right] \end{aligned} \tag{7}$$

where $\overline{B_\parallel}$ is the mean geomagnetic field during the RO. The second term on the right-hand-side (RHS) of Eq. (7) represents the residual STEC due to the second-order ionospheric effect and will be accounted for in our calculations. Such a linear combination neither has previously been discussed, nor have STEC values free from the second-order ionospheric effect been previously reported, either for GPS ground-based or RO measurements. The third term in the brackets in the RHS of Eq. (7) describes the residual STEC due to the combination of the carrier-phase ambiguities, GPS and LEO inter-frequency biases, multipath and ionospheric noise, and it obtains small values thus, it can safely be omitted when estimating RO STEC. Nevertheless, the uncertainty induced by each term can be associated with a theoretical and/or observational error and could be addressed separately.

The estimation of the second-order ionospheric delay in ground-based GPS experiments involves ionosphere (International Reference Ionosphere; IRI-2007) and geomagnetic field (International Geomagnetic Reference Field; IGRF-10) models. Yet, the source of the second-order ionospheric delay in GPS measurements is the Faraday rotation effect, which causes a phase shift on the received GPS signals [*De Roo et al.,* 2004]. The Faraday rotation is proportional to the square of the electromagnetic wavelength, to the free electron number density in the ionosphere and to the Earth's magnetic field along the GPS signal propagation hence, the second-order ionospheric delay can be expressed as:

$$s_1 = \frac{2\pi m^2 c^4 K\beta}{\lambda^2 e^3 f_1^3} \tag{8}$$

where β is the signal phase shift (radians), λ is the wavelength (m), c is the speed of light in vacuum (m/s), e is the electron charge (C), f_1 is the GPS signal frequency in the L_1 channel, m is the electron mass and K is a constant.

Model results and discussion

Figure 2*a* shows the L_1 and L_2 phase delays as function of time, ranging within [-7, -15] m for a setting RO event occurred on 2 December 2006 at 19:27 h, between COSMIC FM1 and GPS PRN04 satellites. The ionospheric RO event examined herein lasts approximately 23 min, while exhibiting small fluctuations attributed to ionospheric variations, particularly when the GPS signals traverse lower parts of the ionosphere, and to uncorrected receiver clock residual errors [cf. Fig. 2*a*].

Figure 2*b* presents STEC values free from second-order ionospheric effects obtained from our algorithm [cf., Eq. (7)] (black) and fall within [70, 110] TECU. Applying *Syndergaard* [2002] algorithm [cf., Eq. (4)] (red) on the same phase delays, we obtain values within [68, 108] TECU. Applying a linear regression model to the STEC obtained from our algorithm [cf., Fig. 2*b*; black dashed line], we observe that the STEC values increase linearly with time, having an *y*-intercept of 68.4±0.82 TECU and a slope of 0.03±0.001 TECU/s. The differences between our algorithm and *Syndergaard's* [2002] algorithm [cf., Eq. (4)] ranged around ~ 2.8 TECU [cf., Fig. 2*b*; light blue line] and are primarily attributed to the second-order ionospheric term not accounted in *Syndergaard's* [2002] equation. The difference between the two approaches indicates that the second-order ionospheric effect appears to be a slowly varying contribution to the STEC values, more or less proportional to the geomagnetic field and the electron number density along the GPS/LEO signal propagation path.

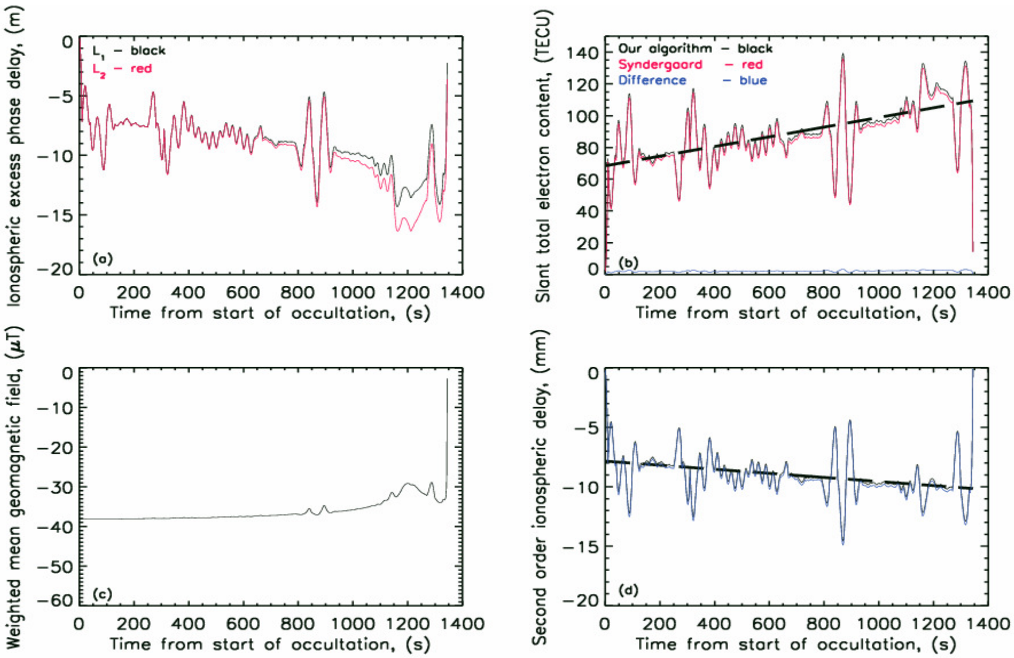

***Figure 2:** (a) L_1 (black) and L_2 (red) raw ionospheric excess phase delays, (b) RO STEC retrieved from our (black), and Syndergaard's, [2002] (red) algorithms and their difference (blue), (c) weighted mean geomagnetic field values and (d) second-order ionospheric delays as function of occultation time computed using the Faraday rotation effect (Eq. 8; blue).*

Figure 2*c* illustrates weighted mean geomagnetic field values as function of time, which we computed as a by product of our research by dividing the results obtained from Eq. (8) with the STEC estimates from Fig. 2*b* (our algorithm; black line). It is shown that the weighted mean geomagnetic field obtains almost a constant value, ranging within [-38, -35] μT, supporting the assumption made by *Syndergaard* [2002], *Kedar et al.* [2003] and *Hoque and Jakowski* [2007], to name a few, of a constant weighted mean geomagnetic field when assessing second-order ionospheric effects in RO STEC and ground-based GPS positioning. The negative sign is due to the fact that the particular RO event was a setting occultation located at ϕ=33.2°S, λ=165.5°W and the direction of the geomagnetic field was opposite to the direction of the GPS signal propagation.

Figure 2*d* demonstrates that the second-order ionospheric delay increases as function of time, obtaining values between -8 mm and -10 mm. Such behaviour is expected, due to the increasing/decreasing electron number density with height above/below the F_2-layer peak. To obtain the behaviour of the second-order ionospheric delay, we apply a linear regression to the retrieved values (dashed black line). The y-intercept and the slope are $-$ 7.85±0.08 mm and $-\ 1.71 \cdot 10^{-3} \pm 1.09 \cdot 10^{-4}$ mm/s. Our results showed that the second-order ionospheric delay obtains larger values than the second-order ionospheric delay estimates for ground-based measurements. This could be attributed to the fact that the GPS signals traverse much longer distance in the Earth's ionosphere during RO events than during ground-based measurements.

Conclusions

This study proposed a new algorithm that retrieves RO STEC accounting for the second-order ionospheric effect and the ray path split between the L_1 and L_2 GPS signals due to ionospheric bending. We demonstrated that the second-order ionospheric delay can be estimated in near-real time by using the Faraday rotation, instead of the standard method which utilizes ionosphere and geomagnetic models.

The ability to estimate accurately both the RO STEC and the second-order ionospheric delay in GPS measurements has wide-ranging implications in the geophysical sciences. A potential application for this type of research may be found in geodetic sciences, where the measurement accuracy of the total electron content (TEC) affects the accuracy of the point positioning. Implementing our proposed techniques into the existing state-of-the-art GPS processing packages such as, BERNESE and GYPSY, we could potentially achieve millimetre accuracy in precise point positioning, which is currently required in numerous geophysical research such as, crustal deformation and plate tectonics motion.

References

Anthes, R. A., P. A. Bernhardt, Y. Chen, L. Cucurull, K. F. Dymond, D. Ector, S. B. Healy, S. –P. Ho, D. C. Hunt, Y. –H. Kuo, H. Liu, K. Manning, C. McCormick, T. K. Meehan, W. J. Randel, C. Rocken, W. S. Schreiner, S. V. Sokolovskiy, S. Syndergaard, D. C. Thompson, K. E. Trenberth, T.-K. Wee, N. L. Yen, and Z. Zeng (2008), The COSMIC/FORMOSAT-3 mission: Early results, *Bull. Am. Meteorol. Soc.*, 89, pp. 313 – 333

Bos, A. G. (2005), Kinematics of the southwestern U.S. deformation zone inferred from GPS motion data, *J. Geophys. Res.*, *110*, B08405

De Roo, R.D., A. W. England, and J. Munn, Circular polarization for L-band radiometric soil moisture retrieval, *Aerospace Conference, 2004. Proceedings. 2004 IEEE*, vol.2, pp. 1015-1023, March 2004

Guier, W. H., and G. C. Weiffenbach (1960), A Satellite Doppler Navigation System, *Proceedings of the IRE,* 48(4), pp. 507–516

Hajj, G. A., L. C. Lee, X. Pi, L. J. Romans, W. S. Schreiner, P. R. Straus, and C. Wang (2000), COSMIC GPS ionospheric sensing and space weather, *TAO*, 11(1), pp. 235–272

Hoque, M. M., N. Jakowski, (2007), Higher order ionospheric effect in precise GNSS positioning, *J. Geod.,* 81, doi:10.1007/s00190-006-0106-0

Kedar, S., G. A. Hajj, B. D. Wilson, and M. B. Heflin, (2003), The effect of the second order GPS ionospheric correction on receiver positions, *Geophys. Res. Lett.,* 30(16), 1829, doi:10.1029/2003GL017639

Longair, M., (1992), High Energy Astrophysics, Vol. 1, 2nd Edition, 440 p. *Cambridge University Press,* New York

Morton, Y. T., Q. Zhou, and F. van Graas (2009), Assessment of second-order ionosphere error in GPS range observables using Arecibo incoherent scatter radar measurements, *Radio Sci.,* 44, doi:10.1029/2008RS003888

Syndergaard, S., (2002), A new algorithm for retrieving GPS radio occultation total electron content, *Geophys. Res. Lett.,* 29(16), 1808, doi:10.1029/2001GL014478

The impact of permafrost disturbances and sediment loading on the limnological characteristics of two High Arctic lakes over four years of study

H. Dugan[1], S.F. Lamoureux, M.J. Lafrenière & T. Lewis
Department of Geography, Queen's University, Kingston, ON K7L 3N6
[1]Email: 4hd2@queensu.ca

INTRODUCTION

Lakes are natural sentinels of long-term environmental change. By integrating upstream terrestrial processes, the chemical and physical characteristics of lakes present a broad indication of local and regional change (Williamson et al. 2008). In small watersheds, large lakes may display resilience to shifts in catchment processes, and maintain a steady-state equilibrium. Similarly, if lake characteristics abruptly change, it may be a signal of a significant regime shift.

It is known that the Arctic is undergoing substantial climatic changes. Rising temperatures will increase active layer thickness and greater rainfall will enhance sediment, geochemical and nutrient fluxes into downstream lakes (Prowse et al. 2006). Long-term monitoring of terrestrial-aquatic linkages is crucial to understanding watershed processes and forecasting environmental changes (Williamson et al. 2008).

In the Canadian Arctic, there is a lack of multi-year monitoring of limnological and hydrological systems. Due mainly to logistical constraints, most research documents a single melt season. Recently, a number of baseline studies have attempted to overcome this shortage by documenting the physical and chemical limnological characteristics of lakes spatially (Antoniades et al. 2003). However, there remains a shortage of temporal limnological studies.

The Cape Bounty Arctic Watershed Observatory (CBAWO, 74°55'N, 109°35'W), located on the south-central coast of Melville Island, has been the site of ongoing inter-disciplinary research in the Earth sciences since 2003. A major goal of the research station is to study the seasonal variability of hydrological and limnological processes in the Canadian High Arctic. The two lakes at the CBAWO have been studied from 2003-2009, which comprises one of the longest Arctic freshwater data sets available. This study focuses on the changing limnological conditions in the two lakes from 2006-09, which have occurred as a result of climatic and catchment disturbances.

STUDY SITE

CBAWO is delineated by paired watersheds, West and East, which feed into two coastal lakes. West and East River are fed primarily by snowmelt, which typically begins in mid-June. By early July, discharge is minimal, but late season floods can be generated by large precipitation events (Dugan et al. 2009). Neglecting transient meltwater tracks, the West River is the sole inflow into West Lake, and drains the 8.0 km^2 West watershed. Likewise, the East River is the sole inflow into East Lake from the 11.6 km^2 East watershed. The lakes are broadly similar, with surface areas of 1.5 km^2, maximum depths of 30-33 m, and ten month ice covers up to 2.3 m thick.

METHODOLOGY

From 2006-09 on West Lake, and 2008-09 on East Lake, vertical profiles of water column properties were taken at three day intervals in 2006-08, and six day intervals in 2009. A Richard Brancker Research XR-420-CTD recorded conductivity (±0.003 mS/cm), temperature (±0.002°C), turbidity (<±2%), and dissolved oxygen (±1%). Additionally, HOBO U22-001 (±0.2°C) water temperature loggers were moored 1 m above the lake bottom.

Water samples for chemical analysis were obtained throughout the water column using a 2 L Kemmerer water sampler. Samples were collected in 1 L Nalgene bottles, and filtered within three hours of sampling. For dissolved organic carbon (DOC) and total dissolved nitrogen (TDN) analyses, water was vacuumed filtered through pre-combusted glass fibre filters, and analysed using high temperature combustion and NDIR and chemiluminescent detection on a Shimadzu TOC-VPCH/TNM system. For dissolved inorganic ion analyses, samples were vacuum filtered with 0.22 μm polycarbonate membrane filters and analysed on a Dionex ICS 300 ion chromatographer. A total data set that included Cl^-, SO_4^{2-}, Na^+, Mg^{2+}, Ca^{2+}, TOC, TN, total dissolved solids (TDS), and turbidity was formed with 192 lake water samples. A principal component analysis (PCA) by the use of a correlation matrix was applied to understand the variability in the data set. Synthetic scores were generated using the factor coefficients of the principal components.

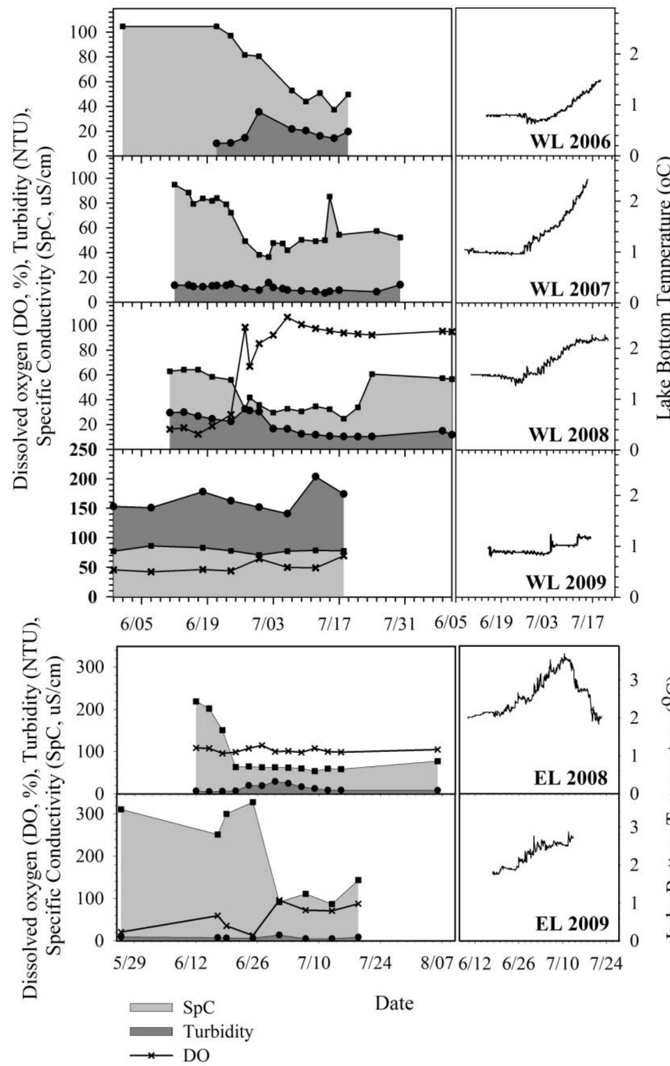

Fig 1. Specific conductivity, turbidity, dissolved oxygen, and temperature at the bottom of West (32 m, 2006-09), and East Lakes (30 m, 2008-09), from CTD profiles. Bottom water temperature recorded from loggers moored at the lake bottom. Note: WL 2009 turbidity was taken from 31 m, as 32 m was extremely high and variable (up to 600 NTU).

RESULTS

West and East Lake are cold-monomictic lakes. Prior to ice melt both lakes both lakes lack stratification with the exception of a thin nepheloid layer at the lake bottom. The lower 1 m or less has higher turbidity and conductivity than the surrounding water column. As the nival freshet begins, melt water is delivered into both lakes. In all years, but West Lake 2009, the high conductivity bottom water is removed at the onset of melt. This period is characterised by a drop in conductivity, a rise in dissolved oxygen, and a small spike in turbidity (Fig 1). After removal of the high conductivity bottom water, the lake bottom temperature begins to rise (Fig 1). By late June, the nepheloid layer is removed, and turbidity is constant throughout the water column. The temperature will rise ~1^{o}C throughout July.

In 2009, the water column in West Lake had significantly elevated TDS and turbidity levels (Fig 2). At depth, the turbidity was ~500 NTU (not shown); 10-fold the value seen in all previous years. During the melt season, the high conductivity bottom water was not flushed, dissolved oxygen remained low, and the lake bottom temperature rose minimally.

A principal component analysis (PCA) on the major ions, nutrient and turbidity levels in both lakes reveal two major components. The first principal component (PC1) is controlled by Cl^-, Na^+, Mg^{2+}, Ca^{2+}, and TDS and describes 66% of the variation in the data set. The second major component (PC2) explained 21% of the total variance. While overall component loading is lower than PC1, PC2 is controlled by TOC, TN, and turbidity. Therefore, PC1 represents ionic strength and PC2 represents the nutrient and sediment concentrations of the samples. Individual PCA scores show a trend of increasing ionic strength over the recorded years for both lakes (Fig 3). West Lake 2009 was the only year that had substantially higher PC2 scores.

DISCUSSION

Over the years of study, West Lake and East have displayed an annual cycling of bottom water. Throughout the winter, high conductivity bottom water builds up and becomes stagnant at the lake bottom. During the nival freshet, quasi-continuous

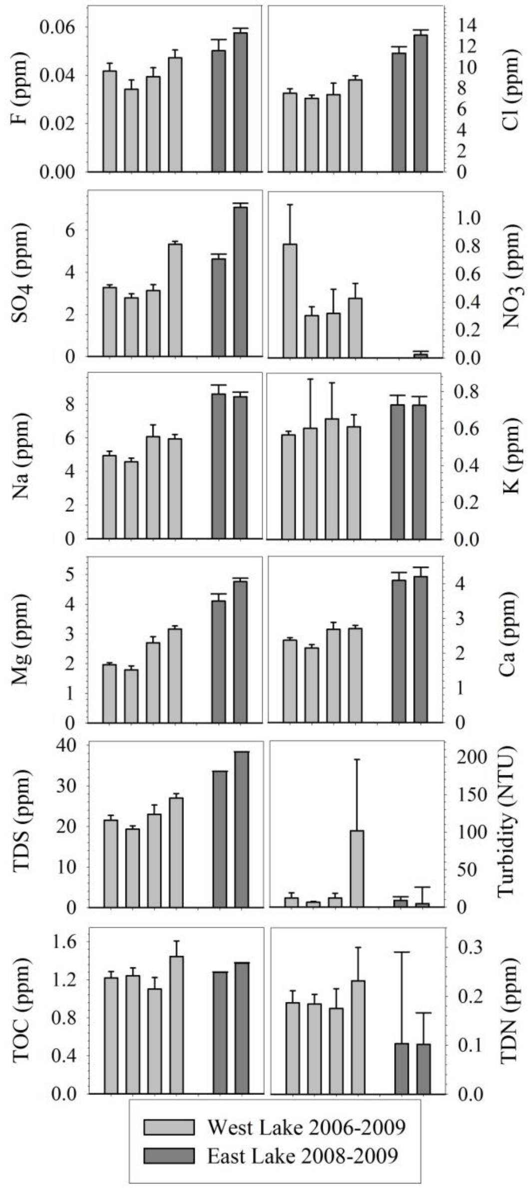

Fig 2. Mean ionic/nutrient (TOC, TDN) concentrations, and turbidity levels in West (2006-29) and East Lakes (2008-09). Error bars equal one standard deviation.

hyperpycnal currents are generated when river water is discharged into the lake. In both lakes, the lack of stratification and cold water allows hyperpycnal flows to easily develop. Inflowing river water must be warmed only minimally, or have a low concentration of suspended sediment to overcome the density of the ambient lake water (Mulder and Alexander 2001). When underflows occur, fresh oxygenated water is delivered to the lake bottom. This replenishment of oxygen is critical to the benthic ecosystems in these lakes. Known biota include arctic char, and benthic

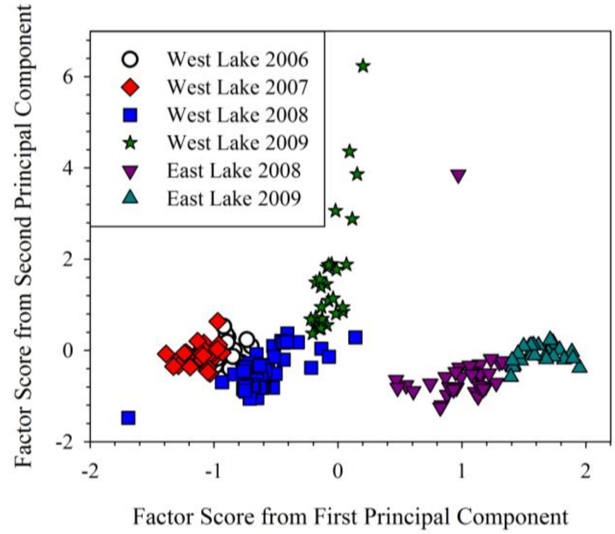

Fig 3. PCA scores for West (2006-09) and East Lakes (2008-09. PC1 represents ionic strength, and PC2 is associated with turbidity and nutrient levels.

amphipods (unconfirmed as *Gammarus lacustris*, T. Lewis *pers. comm*.).

There have been two major developments in the limnological characteristics of West and East Lake over the study years. The first is a trend towards high TDS throughout the water column, and the second is a major sediment delivery into West Lake that perturbed annual cycling.

Increasing ionic strength in West and East Lake

In Arctic nival rivers and lakes, the majority of flow occurs from snowmelt. Because solute concentrations in snow are extremely low, and there is minimal interaction between nival runoff and the frozen permafrost, solute concentrations tend to be low in downstream lakes. The highest solutes levels in Arctic catchments are found in near-surface ground ice and permafrost (Kokelj et al. 2009).

When permafrost degrades, soluble ions are released into the active layer, and become susceptible to removal by throughflow. In a study of 73 ponds and lakes affected by thermokarst disturbance in the Mackenzie Delta Region, there was a strong correlation between thaw slumping and ionic concentration of lakes (Kokelj et al. 2009). Additionally, the ionic concentrations in previously slumped soils were above non-disturbance controls, indicating that thaw slumping of permafrost may impact downstream fluxes for decades following the initial slump (Kokelj et al. 2005).

In previous studies of the limnological characteristics of Arctic lakes, including both baseline monitoring (Antoniades et al. 2003) and the chemical composition of disturbed lakes (Kokelj et al. 2005; Kokelj et al. 2009), the study lakes were relatively small and shallow; many less than 5 m deep. In many regions, these small ponds are ubiquitous across the landscape, and their shallow nature imparts a high sensitivity to external perturbations (Antoniades et al. 2003).

Our study lakes have a much larger volume than the aforementioned ponds, and therefore, are indicators of larger, and potentially long-term, changes in catchment fluxes. PCA results illustrate broad groupings of lake samples over a number of years. Our results of a PC1 associated with ionic strength, and PC2 associated with nutrient levels, is similar to the results of other High Arctic studies looking at limnological characteristics across space (Antoniades et al. 2003).

The scores from PC1 show the development of increasing conductivity in both West and East Lake. From 2006 to 2007 the overall conductivity of West Lake decreased, but between 2007 and 2008, and 2008 and 2009 in both lakes, there was a significant rise in TDS. In both lakes, there was a consistent rise in F^-, Mg^{2+}, NO_3^-, Cl^-, and a large rise in SO_4^{2-} (Fig 2).

This trend began concurrently with large active layer disturbances in the CBAWO in 2007. In July 2007, the erosion of loose surficial material led to high levels of turbidity in the catchment rivers. At the time, it was hypothesized that the availability of erodible material would have a sustained impact on sediment and chemical fluxes in the watershed for a number of years (Lamoureux and Lafreniere 2009). The initial thickening of the active layer, melting of ground ice, and continued availability of sediment clearly increased the ionic loading of the two lakes. In both catchments, river discharge is typically between 0.6 to 1.2 million m^3 over the melt season (Dugan et al. 2009). On the higher end, this only accounts for approximately 5.5% of the total volume of the individual lakes. Therefore, the rise in TDS in both watersheds must have risen considerably to account for the significant increase seen in both lakes.

Furthermore, there was a slight, yet significant decrease in TOC levels between 2007 and 2008 in West Lake ($p=0.002$). This is similar to a drop in DOC observed in the thermokarst lakes on the Mackenzie Delta. This initial change in TOC may be a result of retention of DOC through sorption by a thickening active layer in late 2007 (Kokelj et al. 2005). In 2008, the active layer deepening was thin in comparison to 2007, and TOC levels in 2009 were higher than 2008.

Elevated turbidity in West Lake 2009

PC2 scores for West Lake 2009 reveal a substantial departure from all other years. The quantity of sediment delivered into the lake between Aug 2008 and May 2009 is approximately 127 Mg. This value is moderate in comparison to the seasonal sediment loads of West River from 2004-2007, which varied between 63 and 447 Mg. In 2007, two large precipitation events only liberated 41 and 43 Mg of sediment individually (Dugan et al. 2009). While there has been elevated sediment availability in the West watershed as a result of active layer detachments, there is no terrestrial mechanism to generate this degree of sediment loading. In 2007 there was minimal precipitation; much below levels necessary to reactivate rivers in the autumn. Additionally, there was no apparent disturbance near the edge of West Lake that could have delivered sediment directly into the water body. One mechanism for high turbidity in the water column is an internal disturbance in West Lake. It is possible that a surge-type current could have been generated from internal basin slumping. These slides can be initiated on delta fronts where sediment has accumulated from river inflows.

The high turbidity levels effectively prevented the annual mixing cycle in West Lake. In the four years presented for West Lake and the two years for East Lake, this is the only documented case where the anoxic, high conductivity water that built up over the winter was not removed during spring melt. Additionally, the high turbidity initiated thermal stratification and prevented the lake from warming throughout the season.

High suspended sediment levels in northern lakes can have a considerable impact on lake biota. Sediment particles effectively block light transmission, which lowers temperature and food availability. Moreover, the lack of re-oxygenation of bottom water would have been detrimental to the benthic ecosystem in West Lake. In some cold-regions lakes that are extremely oligotrophic, benthos are the primary source of carbon (Sierszen et al. 2003). If this is the situation in West Lake, the entire food web could have been altered by the sediment loading.

Conclusions and future trajectories:

Most freshwater lakes in the world are holomictic; that is, they experience complete mixing of the water-column at least annually. This mixing and refreshing of water is of consequence to lake biota, as turn-over delivers oxygen and nutrients to the lake bottom (Boehrer and Schultze 2008). In 2009, suspended sediment created a density gradient in West Lake that was not destroyed during the nival freshet. This distinct regime shift likely had a large impact on lake biota, as bottom water remained cold and anoxic throughout the season.

If this is assumed to be a stochastic event, the lake will likely return to the aforementioned mixing cycle. More importantly for long-term dynamics, is the trend toward higher ionic concentrations in both West and East Lakes. In the future, the Canadian High Arctic will undergo considerable warming, especially in the fall and winter (Prowse et al. 2006). A hydrological and sediment yield model applied on the West River of Cape Bounty found that by 2100, total annual runoff and daily maximum discharge will double, and the melt season length will increase by 30 days; mostly into the fall. Additionally, minimum estimates of annual sediment yield predict a 100-600% increase (Lewis and Lamoureux 2010). Elevated late-season temperatures will increase active layer thickening and the possibility for large-scale precipitation events. Together, these processes will increase geochemical and nutrient fluxes throughout watersheds; triggering an increase in aquatic productivity. With increased sediment availability, high sediment loading of the lakes and generation of semi-permanent stratification, as in seen in 2009, may become more prevalent. As downstream integrators of catchment processes, Arctic lakes will be important indicators of environmental change.

REFERENCES

Antoniades, D., M. S. V. Douglas, and J. P. Smol. 2003. Comparative physical and chemical limnology of two Canadian High Arctic regions: Alert (Ellesmere Island, NU) and Mould Bay (Prince Patrick Island, NWT). Arch. Hydrobiol. **158:** 485-516.

Boehrer, B., and M. Schultze. 2008. Stratification of lakes. Rev. Geophys. **46:** RG2005. 10.1029/2006rg000210.

Dugan, H., S. Lamoureux, M. J. Lafreniere, and T. Lewis. 2009. Hydrological and sediment yield response to summer rainfall in a small high Arctic watershed. Hydrol. Processes **23:** 1514-1526.

Kokelj, S. V., R. E. Jenkins, D. Milburn, C. R. Burn, and N. Snow. 2005. The influence of thermokarst disturbance on the water quality of small upland lakes, Mackenzie Delta region, Northwest Territories, Canada. Permafrost Periglac. **16:** 343-353.

Kokelj, S. V., B. Zajdlik, and M. S. Thompson. 2009. The impacts of thawing permafrost on the chemistry of lakes across the subarctic boreal-tundra transition, Mackenzie Delta region, Canada. Permafrost Periglac. **20:** 185-199.

Lamoureux, S. F., and M. J. Lafreniere. 2009. Fluvial Impact of Extensive Active Layer Detachments, Cape Bounty, Melville Island, Canada. Arct. Antarct. Alp. Res. **41:** 59-68.

Lewis, T., and S. F. Lamoureux. 2010. Twenty-first century discharge and sediment yield predictions in a small high Arctic watershed. Global Planet. Change **71:** 27-41. 10.1016/j.gloplacha.2009.12.006.

Mulder, T., and J. Alexander. 2001. The physical character of subaqueous sedimentary density flows and their deposits. Sedimentology **48:** 269-299.

Prowse, T. D., F. J. Wrona, J. D. Reist, J. J. Gibson, J. E. Hobbie, L. M. J. Vesque, and W. F. Vincent. 2006. Climate Change Effects on Hydroecology of Arctic Freshwater Ecosystems. AMBIO: A Journal of the Human Environment **35:** 347-358.

Sierszen, M. E., M. E. Mcdonald, and D. A. Jensen. 2003. Benthos as the basis for arctic lake food webs. Aquat. Ecol. **37:** 437-445.

Williamson, C. E., W. Dodds, T. K. Kratz, and M. A. Palmer. 2008. Lakes and streams as sentinels of environmental change in terrestrial and atmospheric processes. Front. Ecol. Environ. **6:** 247-254. doi:10.1890/070140.

Canadian Meteorological and Oceanographic Society
La Société canadienne de météorologie et d'océanographie

Meeting Announcement

45th Congress of the Canadian Meteorological and Oceanographic Society (CMOS)

"Ocean, Atmosphere and the Changing Pacific"

June 5 to 9, 2011

at the

Victoria Conference Centre, Victoria, British Columbia, Canada

Sponsor: Canadian Meteorological and Oceanographic Society (CMOS)

Contact: Nathan Gillett, Canadian Centre for Climate Modelling and Analysis, University of Victoria, PO Box 3065 STN CSC, Victoria, BC, V8W 3V6 Canada; Telephone: +1-250-363-8264, Email: lac@cmos.ca

Website: http://www.cmos.ca/congress2011/

Abstract Submission Deadline: February 11th 2011

This Congress will provide a forum for the discussion and presentation of research pertinent to all disciplines represented by the CMOS membership. These include atmospheric science, oceanography, climate science, cryospheric science, hydrology, biogeoscience and interdisciplinary science. The theme for this Congress "Ocean, Atmosphere and the Changing Pacific" provides a focus for certain scientific and plenary sessions. The scientific program will include over 30 sessions covering a wide range of topics.

OFFICERS OF THE 2010-11 CGU EXECUTIVE COMMITTEE

PRESIDENT: Spiros Pagiatakis, York University
Telephone: (416) 736-2100 ext.20644 Fax: (416) 736-5516 Email: spiros@yorku.ca

VICE-PRESIDENT: Gail M. Atkinson, University of Western Ontario
Telephone: (519) 661-4207 x84207 Fax: (519) 661-3198 Email: gatkins6@uwo.ca

PAST PRESIDENT: John Pomeroy, University of Saskatchewan
Telephone: (306) 966-1426 Fax: (306) 966-1428 Email: john.pomeroy@usask.ca

SECRETARY: Maria Strack, University of Calgary
Telephone: (403) 220-5596 Fax: (403) 282-6561 Email: mstrack@ucalgary.ca

TREASURER: Kathy Young, York University
Telephone: (416) 736-5107 ext.22371 Fax: +001 (416) 736-5988 Email: klyoung@yorku.ca

HYDROLOGY SECTION PRESIDENT: Brian Branfireun, University of Toronto
Telephone: (905) 569-4649 Fax: (905) 828-5273 Email: brian.branfireun@utoronto.ca

GEODESY SECTION PRESIDENT: Patrick Wu, University of Calgary
Telephone: (403) 220-7855 Fax: (403) 284-0074 Email: ppwu@ucalgary.ca

SOLID EARTH SECTION PRESIDENT: Kristy Tiampo, University of Western Ontario
Telephone: (519) 661-3188 x83188 Fax: 519-661-3198 Email: ktiampo@uwo.ca

BIOGEOSCIENCES SECTION PRESIDENT: M. Altaf Arain, McMaster University
Telephone: (905) 525-9140 Ext. 27941 Fax: (905) 546-0463 Email: arainm@mcmaster.ca

AWARDS COMMITTEE CHAIR: Hugh Geiger, Talisman Energy, Calgary
Telephone: (403) 237-1234 Fax: (403) 237-1902 Email: HGEIGER@talisman-energy.com

SCIENTIFIC MEETINGS COORDINATOR: Rod Blais, University of Calgary
Telephone: (403) 220-7379 Fax: (403) 284-1980 Email: blais@ucalgary.ca

NEWSLETTER EDITOR: Ed Krebes, University of Calgary
Telephone: (403) 220-5028 Fax: (403) 284-0074 Email: krebes@ucalgary.ca

GAC GEOPHYSICS DIVISION CHAIR: Philip McCausland, University of Western Ontario
Telephone: (519) 661-2111 x87985 Fax: (519) 661-3198 Email: pmccausl@uwo.ca

---

CGU WEB SITE ADDRESS : http://www.cgu-ugc.ca

***Editor's Note*: ELEMENTS, the newsletter for the Canadian Geophysical Union, is published and distributed to all CGU members twice each year; one Summer issue and one Winter issue. We welcome submissions from members regarding meeting announcements or summaries, awards, division news, etc. Advertisements for employment opportunities in geophysics will be included for a nominal charge (contact the Editor). Notices of post-doctoral fellowship positions available will be included free of charge.**

Submissions should be sent to the Editor:

Prof. E.S. Krebes, Dept. of Geoscience, University of Calgary, Calgary, Alberta, Canada, T2N 1N4. Telephone: (403) 220-5028; Fax: (403) 284-0074; Email: krebes@ucalgary.ca.
Electronic submission is encouraged.

CSAFM Canadian Society of Agricultural and Forest Meteorology
Société canadienne de météorologie agricole et forestière SCMAF

Canadian Geophysical Union
Union Géophysique Canadienne
www.cgu-ugc.ca

Canadian Society of Agricultural
and Forest Meteorogy
Société canadienne de météorologie
agricole et forestière
www.uoguelph.ca/~csafm

ANNUAL MEETING / RENCONTRE ANNUELLE

under the theme

GEOPHYSICAL SCIENCES FOR THE FUTURE

May 15 - 18 Mai, 2011

Banff Park Lodge, Banff, Alberta

Preliminary Technical Program

Geodesy:	Geodesy, Geodynamics, Planetary and Space Sciences, ...
Hydrology:	Hydrology, Cryosphere, Environment, Climate Systems, ...
Solid Earth:	Seismo-Tectonics, Imaging, Natural Hazards and Risks, ...
Biogeosciences:	Biogeosciences, Climatology, Ecosystems, Nutrients, ...
CSAFM:	Canadian Carbon, MicroMeteorology, ...
General:	Advanced Geocomputations, General Geophysics, ...

Workshop & Session Proposals due: 15 November/Novembre 2010
Abstracts / Résumés due: 15 February/Février 2011
Field Trip to Columbia Icefield on 15 May/Mai 2011

More Information: www.ucalgary.ca/~cguconf